IEEE Photonics Journal
An IEEE Photonics Society Publication

Open Access

Determination of Reactive RF-Sputtering Parameters for Fabrication of SiO_x Films With Specified Refractive Index, for Highly Reflective SiO_x Distributed Bragg Reflector

Volume 9, Number 1, February 2017

Elnaz Afsharipour, ***Student Member, IEEE***
Byoungyoul Park, ***Member, IEEE***
Cyrus Shafai, ***Senior Member, IEEE***

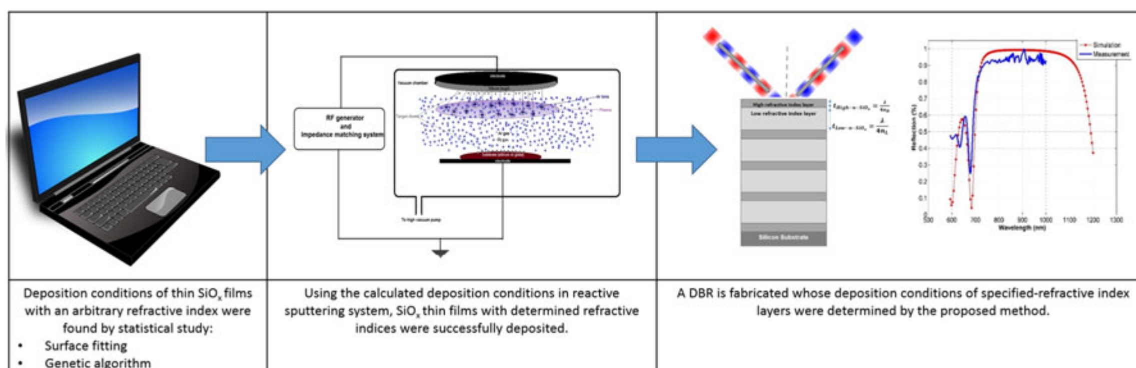

DOI: 10.1109/JPHOT.2017.2649500
1943-0655 © 2017 IEEE

IEEE photonics SOCIETY

IEEE

Determination of Reactive RF-Sputtering Parameters for Fabrication of SiO_x Films With Specified Refractive Index, for Highly Reflective SiO_x Distributed Bragg Reflector

Elnaz Afsharipour, ***Student Member, IEEE,***
Byoungyoul Park, ***Member, IEEE,***
and Cyrus Shafai, ***Senior Member, IEEE***

Department of Electrical & Computer Engineering, University of Manitoba, Winnipeg R3T 2N2, Canada

DOI:10.1109/JPHOT.2017.2649500
1943-0655 © 2017 IEEE. Translations and content mining are permitted for academic research only. Personal use is also permitted, but republication/redistribution requires IEEE permission. See http://www.ieee.org/publications_standards/publications/rights/index.html for more information.

Manuscript received December 15, 2016; accepted January 3, 2017. Date of publication January 9, 2017; date of current version January 24, 2017. This work was supported by the Natural Sciences and Engineering Research Council of Canada. Corresponding author: E. Afsharipour (e-mail: afsharie@myumanitoba.ca).

Abstract: Fabricating materials with specific refractive indices, which do not naturally exist in the nature, has always been an issue. This paper presents a method for fabricating SiO_x films with specified refractive index. It is well known that the refractive index of reactively sputtered SiO_x films depends on its deposition conditions; in this paper, this fact was employed to fabricate films with arbitrary refractive indices. A statistical study and a Genetic Algorithm are implemented that can determine the deposition conditions (including oxygen partial flow and pressure) for fabricating a film with an arbitrary refractive index in the range of 1.4–4.2. The method was experimentally shown to correctly determine the deposition conditions. The functionality of using the proposed method in fabricating optical components was further evaluated by fabricating a distributed Bragg reflector (DBR) consisting of 4.5 pairs, whose refractive indices of the layers were determined by the proposed method. The DBR featured a high 95% reflection in a bandwidth of more than 270 nm, which can be categorized as a high-quality DBR. The advance of the proposed method is that the films are made from a single target source without making any physical changes in the target or substrate positions.

Index Terms: Distributed Bragg reflector (DBR), genetic algorithm, optimization, photonic crystals, photonic materials, refractive index of SiO_x.

1. Introduction

Films with specific refractive indices are extremely important in anti-reflection layers and solar cells; however, fabricating films with specific refractive indices has always been a challenging issue. Creating materials with arbitrary refractive indices that do not inherently exist in nature, has been done by four methods. The first method is fabricating a multi-stack layer structure, composed of higher and lower refractive index materials. When the thickness of each layer is much less than the wavelength of light, the structure can be assumed as a single layer of homogenous material. The equivalent refractive index is calculated using the optical thicknesses of the two

constituent materials. The desired refractive index can be achieved by varying the thickness of layers [1], [2]. This method requires two different materials and accurate calculation of layers thickness configuration. Glancing Angle Deposition (GLAD) [3]–[5] and co-sputtering techniques [2] are the other two methods employed for making films with a specific refractive index. In glancing angle deposition, which is an enhanced form of oblique angle deposition, the porosity of deposited film is controlled by the angle of incident vapor flux and rotation of the substrate. Films with specific refractive indices can be deposited by controlling the porosity. In the co-sputtering method, two or more materials such as SiO_2 and TiO_2 are deposited simultaneously onto a substrate, and the refractive index of final deposited film is controlled by the deposition rate of each material component.

The fourth method is to create a material that possesses the specific desired refractive index. This can be done, for example, by reactive sputtering [6]–[9] or chemical vapor deposition (CVD) [10] methods, in order to form a specific material stoichiometry that possesses a desired refractive index. Unlike the multi-stack layer and co-sputtering method in which two or materials are required, the reactive sputtering of the forth method takes the advantage of depositing material of a single source target, while it can still make a wide range of refractive indices. Khodier *et al.* [11] compared the effect of three deposition methods (chemical vapor deposition, electron beam evaporation, and sputtering) on the refractive index of SiO_2 and showed that sputtered films have the highest refractive index from 1.51–1.59. They mentioned that the formation of non-stoichiometric compounds (like Si, SiO, SiO_x) is the reason for the higher refractive index. Moreover, unlike GLAD deposition, the reactive sputtering method does not need a rotating target or substrate in order to make the appropriate vapor angle. In addition, comparing to thermal evaporation and CVD, sputtering is a low-temperature deposition method, which enables deposition of SiO_x with potentially minimal thermal stress or damaging temperature sensitive substrates.

Reactively sputtered SiO_x films have been explored by various groups. However, to form a specific refractive index, significant effort in calibrating and understanding how a material's refractive index changes with chemical stoichiometry, and the deposition processes parameters is needed. For example, there are differing reports on effect of oxygen partial flow on refractive index of sputtered SiO_2. Wu *et al.* in [7] explored the effect of varying oxygen partial flow when reactively sputtering SiO_2 from a silicon target. The partial flow rate of oxygen with respect to argon flow ($O_2/(O_2 + Ar)$) was varied from 10–20% at 6 mTorr working pressure, and RF power of 100 W. It was found that the refractive index increased from 1.46–1.53, with increasing oxygen flow. In contrast, Chichibu *et al.* in [8], found that increasing the oxygen partial flow decreased the refractive index. In [8], the oxygen partial flow was increased from 10–60% at 1.5 mTorr pressure and RF power of 300 W, and the refractive index was found to decrease from 1.47–1.46.

We can see from the above works that predicting how a change in a reactive sputtering parameter could affect the refractive index of a SiO_x film is challenging. One solution could be mathematical modeling of the deposition process in the sputtering system. Theoretical modeling of the reactive magnetron sputtering processes has been undertaken by various groups [12]–[15]. The model of Palmero *et al.* [12] includes the sputtering model, electron kinetic equations, plasma chemistry model, and electromagnetic model to find the mathematical relation between sputtering parameters and deposited silicon oxide film stoichiometry and the deposition rate. These parametric models are complex, and can be used to determine the parameters like growth rate of a thin film and its final stoichiometry. However, it cannot be used to specifically predict a refractive index.

It should be mentioned that in situ monitoring of the refractive index of a deposited thin film could be achieved by mounting an ellipsometer on a customized sputtering system [16]. However, mounting an ellipsometer requires adding more windows to the sputtering chamber, which can lead to high vacuum difficulties. In addition, since the thickness of the film is increased during the deposition process, the beam alignment and refractive index calculation are also of concern. This would make the in situ optimization of sputtering parameters required to achieve a new (non-calibrated) refractive index, particularly challenging given the many parameters affecting both the reactive sputtering process and refractive index measurement.

In this paper, we demonstrate that prediction of the refractive index of a reactively sputtered film can be done by using an easy to implement statistical model involving only two parameters, pressure and reactive gas partial flow. In this work, three studies were undertaken. First, several reactively sputtered SiO_x thin films were deposited at varying pressure and reactive gas flow, to provide a suitable range of stoichiometry for statistical study. SiO_x was deposited by reactive sputtering from a silicon target by varying the oxygen partial flow between 1% and 11% for three deposition pressure ranges (low range from 1.4–1.7 mTorr, medium range 8.5–10 mTorr, and high range 15–17 mTorr). From this initial effort, a wide range of refractive indices from 1.48 to 4.28 were deposited. Second, the statistical model of how the two sputtering parameters (oxygen partial flow and pressure) affect refractive index is developed. Finally, a genetic algorithm (GA) is employed to predict the required optimum system pressure and oxygen partial flow needed to deposit SiO_x layers with a specified refractive index, from the statistical model. As a demonstration of the effectiveness of this statistical model method, the required deposition conditions needed to fabricate a distributed Bragg reflector (DBR) from alternating layers of high and low refractive index SiO_x is calculated. The fabricated DBR showed a high 95% reflection with a wide flat band of more than 270 nm in the visible and near infrared region from 730 nm–1000 nm.

2. Experimental Details

Silicon wafer substrates (p-type and (100) orientation) were prepared by cleaning in piranha solution (4:1; conc. H_2SO_4/H_2O_2) for 10 minutes to remove organic residues. This was followed by etching in BOE solution (6:1; NH_4F/HF) for 2 minutes to remove native oxide. SiO_x thin films were deposited by a 13.56 MHz RF magnetron sputtering system using an undoped 99.999% pure silicon target in an argon plasma with reactive oxygen gas. The distance between target and substrate was 6 cm and RF power of 200 W was applied in all the experiments. The deposition time was 10 minutes. The base pressure of the deposition chamber was 3.7×10^{-6} Torr before deposition was started. The flow rate of high purity argon and oxygen gases introducing into the chamber was controlled by mass flow controllers.

The experiment was conducted at three pressure ranges, low range from 1.4–1.7 mTorr, medium range from 8.5–10 mTorr and high range from 15–17 mTorr. For each pressure range, six samples were deposited by varying the oxygen partial flow between 1 to 11%. The experiments were designed so that only one parameter was changing while the other parameters were kept constant. The oxygen partial flow and the deposition pressure range were selected based on values reported in [7], [8], [12], [17]–[19], in order to cover a wide range of reasonable deposition conditions. A total of 18 SiO_x samples were deposited. The deposition parameters are summarized in Table 1. The refractive index of the films was measured using an M-2000D J.A.Woolam ellipsometer at a reference wavelength of 632.8 nm, which is considered as a standard wavelength of refractive index measurement [20]. Since the imaginary part of refractive index in dielectrics is almost zero, they have very low losses in optical and near infrared wavelengths [21], so the losses were neglected in this study. In all the experiments, three different points on each sample were measured and the average value was recorded.

The variation of the refractive indices of the experimentally deposited SiO_x films versus pressure are shown in Fig. 1. We can see that at a given oxygen partial flow, increasing the system pressure, resulted in a smaller refractive index. This trend was almost true for all oxygen partial flow levels from 1% to 11%. Since the mean free path is shorter at higher pressures, there are a larger number of collisions between target atoms and gas molecules. According to [7] and [22], this can cause more porosity which then reduces the refractive index.

Fig. 2 illustrates the variation of the refractive index of the deposited films versus oxygen partial flow, at three different pressures. We can see that for low and medium system pressures, the higher oxygen partial flow reduces the refractive index. As the oxygen partial flow increases, there are more available oxygen atoms to react with the silicon atoms. The effect of oxygen partial flow is very significant at lower deposition pressures [see Fig. 2(a)]. The slope is smoother at medium pressures [see Fig. 2(b)]. In contrast, at higher deposition pressures even small amounts of oxygen

TABLE 1
Deposition Parameters and Measured Refractive Index of Sputtered SiO_x Films for 18 Different Samples

Pressure Range	Sample	Ar flow rate (sccm)	O_2 flow rate (sccm)	$O_2/(O_2 + Ar)$	Pressure (mTorr)	Refractive index
High	**1**	80	0.8	1%	15	1.51
	2	80	2.5	3%	16	1.52
	3	80	4.2	5%	16	1.53
	4	80	6.0	7%	16	1.49
	5	80	7.9	9%	17	1.48
	6	80	9.9	11%	17	1.49
Medium	**7**	50	0.5	1%	8.5	2.03
	8	50	1.5	3%	9	2.00
	9	50	2.6	5%	9.1	1.48
	10	50	3.8	7%	9.2	1.49
	11	50	4.9	9%	9.7	1.50
	12	50	6.2	11%	10	1.50
Low	**13**	20	0.2	1%	1.4	4.28
	14	20	0.6	3%	1.5	3.30
	15	20	1.1	5%	1.5	3.40
	16	20	1.5	7%	1.4	3.37
	17	20	2.0	9%	1.6	3.08
	18	20	2.5	11%	1.7	2.07

($O_2/(O_2 + Ar) = 1\%$) results in a very low refractive index, and therefore, the slope is almost constant (with small fluctuations) [see Fig. 2(c)]. This result also correlates with the research done by Wu *et al.* in [7].

3. Statistical Model for Refractive Index Determination

Table 1 shows that the refractive index of the deposited film can vary through a wide range, depending on the process parameters of oxygen partial flow and pressure. In order to predict the process for an arbitrary refractive index, a relationship between the deposition parameters and refractive index needs to be established. This was done by applying a 3-D surface, since we are relating two variables (oxygen partial flow and pressure) and refractive index. This 3-D surface is in effect a statistical model of knowledge gained from prior processes.

Determining the deposition parameters to make a film with a new (previously not deposited) refractive index from the statistical model, was done using a genetic algorithm. A genetic algorithm (GA) was used since it is an established method in finding optimized solutions, and it can calculate this in a short time. GA have been used by various groups to optimize sputtering system parameters for depositing different materials [23]–[25]. For example, Lin *et al.* [23] implemented a GA to determine the nitrogen flow rate and sputtering power for fabricating films with specific absorption coefficient in solar cells. They have concluded that their proposed method can save time and energy in the process line of solar cell manufacturing. In this work, the oxygen partial flow and pressure

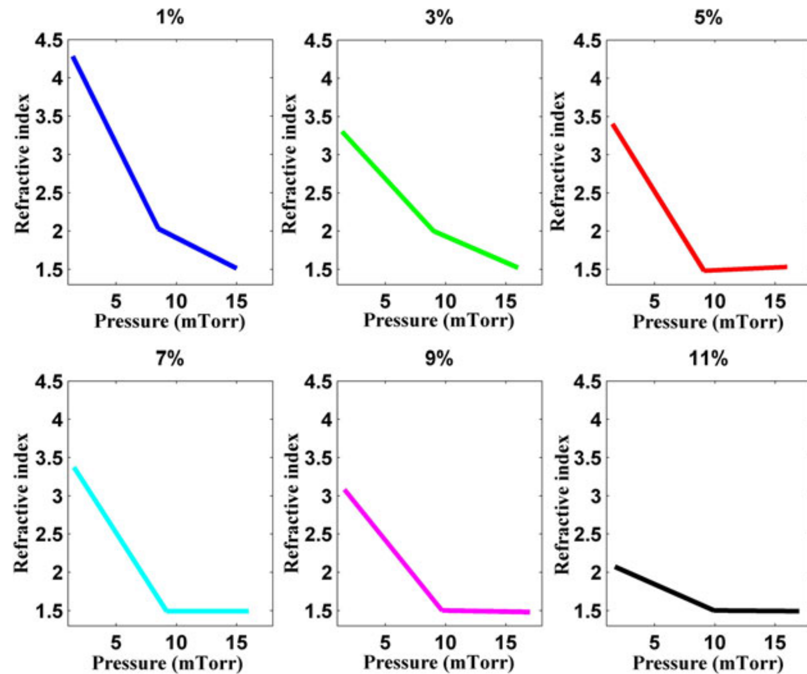

Fig. 1. Measured refractive index of sputtered SiO_x versus deposition pressure for different oxygen partial flows ($O_2/(O_2 + Ar) = 1\%$ to 11%).

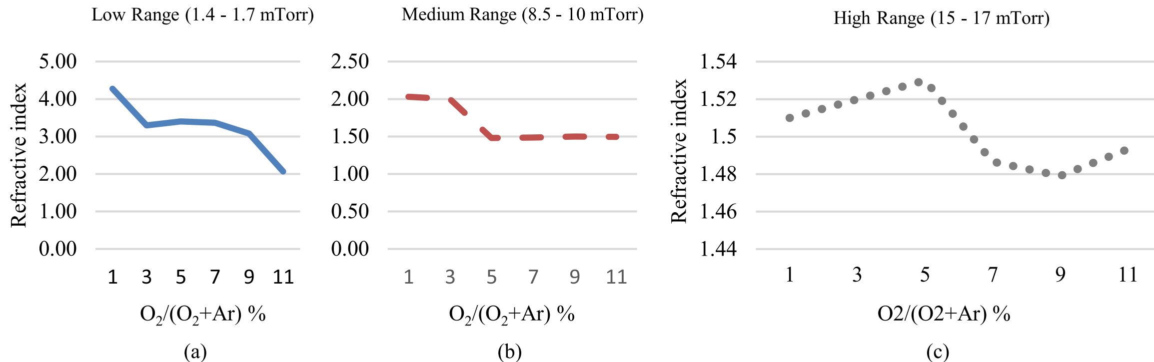

Fig. 2. Measured refractive index of sputtered SiO_x versus oxygen partial flow in three different pressure levels.

are the process parameters that will be determined for fabricating a film with a specified refractive index.

3.1 Surface Fitting

A polynomial regression method was implemented to determine the 3D fitness function surface, with the assumption that a polynomial of degree 2 for both the process variables will suitably represent the surface. The accuracy of this assumption will be discussed later. The following equation (1) shows the polynomial relation for the fitness function:

$$\hat{z} = p_{00} + p_{10}x + p_{01}y + p_{20}x^2 + p_{11}xy + p_{02}y^2 \tag{1}$$

where x represents the oxygen partial flow, y represents the pressure, $\hat{z}$ represents the calculated refractive index, and the six coefficients of the polynomial terms are p_{00}, p_{10}, p_{01}, p_{20}, p_{11}, p_{02}.

The six coefficients of the fitness function can be found using a least square method that calculates the deviation between predicted ($\hat{z}_i$) refractive index (for each data point in Table 1) and measured values (z_i) of the refractive index. Performing this over all experimental data points in Table 1, we have a Sum of Squared Errors (SSE) as

$$\mathrm{SSE} = \sum_{i=1}^{n} (z_i - \hat{z}_i)^2 \tag{2}$$

where z_i is the observed value of refractive indices (from Table 1), $\hat{z}_i$ is the predicted value (fitted value), and n is the number of experiments in Table 1. Substituting $\hat{z}_i$ in the SSE we have

$$\mathrm{SSE} = \sum_{i=1}^{n} \left(z_i - \left(p_{00} + p_{10}x_i + p_{01}y_i + p_{20}x_i^2 + p_{11}x_iy_i + p_{02}y_i^2\right)\right)^2. \tag{3}$$

The coefficients can be found by taking the partial derivative of the SSE equation with respect to each of the coefficients, and setting this to zero. This is illustrated for the first coefficient as follows:

$$0 = \frac{\partial \mathrm{SSE}}{\partial p_{00}} = \sum_{i=1}^{n} (-2)(z_i - p_{00} - p_{10}x_i - p_{01}y_i - p_{20}x_i^2 - p_{11}x_iy_i - p_{02}y_i^2). \tag{4}$$

Solving, we obtain

$$\sum_{i=1}^{n} z_i = np_{00} + p_{10}\sum_{i=1}^{n} x_i + p_{01}\sum_{i=1}^{n} y_i + p_{20}\sum_{i=1}^{n} x_i^2 + p_{11}\sum_{i=1}^{n} x_iy_i + p_{02}\sum_{i=1}^{n} y_i^2. \tag{5}$$

Similarly, we can find the partial derivatives of the other five coefficients.

$$\begin{aligned}\sum_{i=1}^{n} zx_i = p_{00}\sum_{i=1}^{n} x_i + p_{10}\sum_{i=1}^{n} x_i^2 + p_{01}\sum_{i=1}^{n} x_iy_i \\ + p_{20}\sum_{i=1}^{n} x_i^3 + p_{11}\sum_{i=1}^{n} x_i^2y_i + p_{02}\sum_{i=1}^{n} x_iy_i^2\end{aligned} \tag{6}$$

$$\begin{aligned}\sum_{i=1}^{n} z_iy_i = p_{00}\sum_{i=1}^{n} y_i + p_{10}\sum_{i=1}^{n} x_iy_i + p_{01}\sum_{i=1}^{n} y_i^2 \\ + p_{20}\sum_{i=1}^{n} x_i^2y_i + p_{11}\sum_{i=1}^{n} x_iy_i^2 + p_{02}\sum_{i=1}^{n} y_i^3\end{aligned} \tag{7}$$

$$\begin{aligned}\sum_{i=1}^{n} z_ix_i^2 = p_{00}\sum_{i=1}^{n} x_i^2 + p_{10}\sum_{i=1}^{n} x_i^3 + p_{01}\sum_{i=1}^{n} y_ix_i^2 \\ + p_{20}\sum_{i=1}^{n} x_i^4 + p_{11}\sum_{i=1}^{n} x_i^3y_i + p_{02}\sum_{i=1}^{n} y_i^2x_i^2\end{aligned} \tag{8}$$

TABLE 2
Coefficients of Polynomial of (1), Found by Minimizing the Sum of Squared Errors

p_{00}	p_{10}	p_{01}	p_{20}	p_{11}	p_{02}
4.697	−0.2	−0.4	0.007	0.005	0.013

$$\sum_{i=1}^{n} z_i x_i y_i = p_{00}\sum_{i=1}^{n} x_i y_i + p_{10}\sum_{i=1}^{n} x_i^2 y_i + p_{01}\sum_{i=1}^{n} x_i y_i^2 + p_{20}\sum_{i=1}^{n} x_i^3 y_i + p_{11}\sum_{i=1}^{n} x_i^2 y_i^2 + p_{02}\sum_{i=1}^{n} x_i y_i^3 \quad (9)$$

$$\sum_{i=1}^{n} z_i y_i^2 = p_{00}\sum_{i=1}^{n} y_i^2 + p_{10}\sum_{i=1}^{n} x_i y_i^2 + p_{01}\sum_{i=1}^{n} y_i^3 + p_{20}\sum_{i=1}^{n} x_i^2 y_i^2 + p_{11}\sum_{i=1}^{n} x_i y_i^3 + p_{02}\sum_{i=1}^{n} y_i^4. \quad (10)$$

We now have six equations, which can be used to solve for the six coefficients. Solving (5) to (10) in MATLAB, the six coefficients were obtained and are shown in Table 2. Substituting the coefficients of Table 2 into (1), we obtain the final fitness function shown in (11), which is plotted in Fig. 3.

$$\hat{z} = 4.697 - 0.2*x - 0.4*y + 0.007*x^2 + 0.005*xy + 0.013*y^2. \quad (11)$$

The validity of the assumption that a polynomial degree of 2 for both the process variables in the fitness function should be considered. This can be done by considering the coefficient of determination R^2 of (12), shown below, between the SSE for each refractive index data point on Table 1, and the total sum of the squared differences of each data point (in Table 1) compared to the mean of the data (TSS):

$$R^2 = 1 - \frac{SSE}{TSS} \quad (12)$$

$$TSS = \sum_{i=1}^{n} (z_i - \bar{z})^2 \quad (13)$$

$$\bar{z} = \frac{1}{n}\sum_{i=1}^{n} z_i \quad (14)$$

where z_i is each observed value from Table 1, and $\bar{z}$ is the mean of all observed data.

The coefficient of determination (R^2) provides a measure of how much the found fitness function deviates from the experimental data points. The higher the R^2, the closer the fitted surface

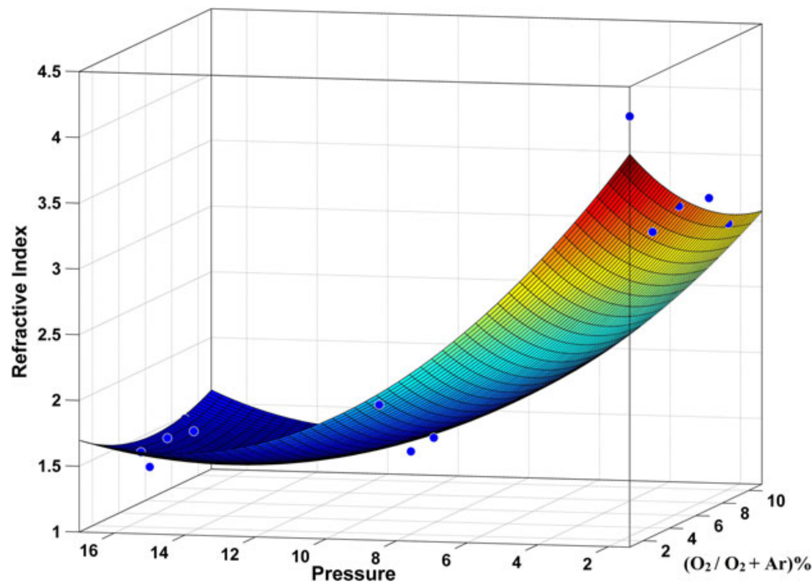

Fig. 3. Plotted fitness function of (11). Blue dots show the experimental data points of Table 1.

TABLE 3
Fitted Models Using Polynomials of Various Degrees for Oxygen Partial Flow (x) and Pressure (y), Showing the SSE and R^2

x degree	*y* degree	SSE	R^2	Model
1	1	3.12	0.74	$z = p_{00} + p_{10}*x + p_{01}*y$
2	1	2.41	0.77	$z = p_{00} + p_{10}*x + p_{01}*y + p_{11}*x*y + p_{20}*x^2$
1	2	0.41	0.96	$z = p_{00} + p_{10}*x + p_{01}*y + p_{11}*x*y + p_{02}*y^2$
2	2	0.34	0.96	$z = p_{00} + p_{10}*x + p_{01}*y + p_{11}*x*y + p_{20}*x^2 + p_{02}*y^2$

is to the observed data. Using (1), polynomials with different degrees (1 or 2) for x and y can by explored by setting these respective coefficients to zero, and resolving the fitness function polynomial. Table 3 shows the calculated SSE and R^2 for the fitness function for the cases of polynomials with degrees of 1 and 2 considered for variables x (oxygen partial flow) and y (pressure). We can see the fitness function of order 2 for x and y provides the best fitness function compared to lower order polynomials. It should be mentioned, that higher order polynomials of degree 3 and 4 were also explored, however, it was found that the R^2 did not significantly change.

Two other fitting methods were considered in addition to polynomial regression. They were Interpolation and Locally Weighted Scatter plot Smooth (LOWESS), but these were rejected for the following reasons. Interpolation was determined to be not appropriate for predicting the response of new set of variables, since the data has scattered (or non-predictable) error. In the case of LOWESS, a well-fitted curve would result, however, a single equation function (which would serve as a fitness function) cannot be obtained. This would make the implementation of the subsequent GA not straightforward.

Fig. 4. Stochastic Universal Sampling technique for selecting the population members as crossover parents for next generation.

3.2 Implementing the GA

Genetic algorithm optimization was implemented using (11) as the fitness function. The GA works to find the local minimum of the fitness function $\hat{z}$, subject to a desired refractive index goal set as the objective value ($n_{objective}$) [26], [27]. The goal is to find the needed deposition parameters where the following equation is met.

$$\hat{z} = \mathrm{n}_{\mathrm{objective}}. \tag{15}$$

Equation (15) is rewritten in the form of (16), shown below, and the GA works to evolve towards the solutions where $S = 0$.

$$\mathrm{S} = \hat{z} - \mathrm{n}_{\mathrm{objective}}. \tag{16}$$

The GA was run generating a population (P) of members of size m. For each population member (P_i) genes for oxygen partial flow (x_i) and pressure (y_i) are randomly selected from between the lower and upper bounds of the oxygen partial flow (1–11%) and pressure (1–20 mTorr). This population group is the 0th generation. The predicted refractive index $\hat{z}_i$ (fitness value) is calculated using (11) for all population members. Equation (16) is then calculated for each population member to check how far the fitness value is from the objective value ($n_{objective}$), which is the base of ranking (scoring) system between population members. Next, the two highest ranking population members to the objective value (those with the smallest score or $|S|$) directly move to next generation. These members are called elite members. The remaining members of the evolution population (p) which now has size m-2, are selected as parents for making children of next generation by crossover or mutation methods. The crossover and mutation methods are performed to make children equal in number to 80% and 20% of the evolutionary sub-population, respectively. The selection of 80% and 20% is a common implementation ratio [28], [29].

3.2.1 Crossover Method and Selection for Next Generation: The crossover method uses pairs of parents to generate children for the subsequent generations by combining the genes from the parents, effectively seeking to evolve genes towards superior children. Selection of members for crossover was determined by Stochastic Universal Sampling (SUS) technique [26], which tends to favor selection of unique individuals. First, all the evolution population members (which number p_{m-2}) are placed along a line (see Fig. 4) based on their absolute value deviation ($|S_i|$) from the desired fitness value ($n_{objective}$). The first population member of this group (p_1) is spaced a distance $|S_1|$ from 0. The second evolutionary population member (p_2) is spaced a distance $|S_2|$ from member p_1, thus a total distance $|S_1| + |S_2|$ from 0, and so on for all evolutionary population members. Along this line, each evolutionary population member is given ownership to the line segment to its left.

Next crossover selection is done. A random position along the line of Fig. 4 is selected, and the member who owns the line segment of this position is designated as crossover parent A. The second parent is determined as follows. First a random step size is selected and this is added to the position location of the first parent. The second parent is then found at this new location. If this location is beyond the position of the last evolutionary population member (p_{m-2}), the distance continues to be measured from 0. In essence, the line is actually a circle which wraps back upon itself. The crossover process continues until the number of parent pairs equals 80% of the evolutionary population size, or in other words, $0.8 * (m\text{-}2)$ times.

TABLE 4
GA Parameters for Three Population Size of 10, 15 and 20, With the Objective Being an SiO_x Film With n = 1.45

Case No.	Population size	Evolved generations	Predicted refractive index by GA	*x* (oxygen partial flow)	*y* (pressure)
1	10	7	1.45	8.52	15
2	15	9	1.45	8.55	17.36
3	20	10	1.45	8.53	15.08

Once the parent pairs are selected their genes are mixed to form a child for the next generation. The algorithm used calculates a weighted average of each gene (x and y), with the weighting being a randomly assigned value W from 0 to 1. Equations (17a) and (17b), shown below, show the relation between the generated gene and its parents in the employed crossover method.

$$x_{new} = (1 - W) * x_{parent1} + W * x_{parent2} \quad (17a)$$

$$y_{new} = (1 - W) * y_{parent1} + W * y_{parent2}. \quad (17b)$$

3.2.2 Mutation Method: The mutation method uses a mutated single parent to create a new child. By doing so, this method seeks to randomly create new population members that might potentially have fitness values closer to the objective value. Then augments the crossover method by introducing new genes into the population. In mutation a random change is made to both the genes x and y in a single parent. The random change is done by adding a random vector (V) from a Gaussian distribution within the boundaries of each variable x and y. The new genes are generated using

$$x_{new} = V + x_{parent1} \quad (18a)$$

$$y_{new} = V + y_{parent1}. \quad (18b)$$

3.2.3 GA Convergence Criteria: The GA evolutionary process terminates when the average deviations of fitness values between all members of the population from the objective value ($|S_i|$) is less than the tolerance, which was set to 10^{-4}.

3.2.4 GA Prediction Results: The GA was run to determine the optimal deposition parameters for the goal of $n_{objective} = 1.45$. Table 4 shows the results for three population sizes of $m = 10$, 15 and 20, which were found to evolve to convergence in 7, 9 and 10 generations respectively. The evolution trend of case 3 of Table 4 is illustrated in Fig. 5(a) and (b) as an example. Fig. 5(a) shows the genes (x and y) of all population members in each generation. Fig. 5(b) shows the values of the fitness function for all population members, for each generation.

3.3 Experimental Verification of the GA Results

The optimum values of cases 1 and 2 of Table 4 for x and y were used to reactively sputter new SiO_x thin film samples. The deposition conditions as well as measured refractive index of the new samples are summarized in Table 5. We can see that the measured refractive indices for the deposited films using the GA found conditions of cases 1 and 2 show high correlation with the refractive index value of 1.45, used as the GA's objective value. Previously in Table 1, no thin film was experimentally deposited with a refractive index below 1.48. Therefore, the results of Table 5 clearly show the potential of the GA to predict the needed deposition parameters to deposit a thin film with a refractive index outside of the initial data set of Table 1.

TABLE 5
Sputtering Parameters and Measured Refractive Index of Deposited Samples With GA Predicted Oxygen Partial Flow and Pressure

	$O_2/(O_2+Ar)$	Pressure (mTorr)	Predicted refractive index	Measured refractive index
Table 4 case 1	8.5	15	1.45	1.455
Table 4 case 2	8.5	17.3	1.45	1.44
$n = 2.5$ case	10.2	1.7	2.5	2.513

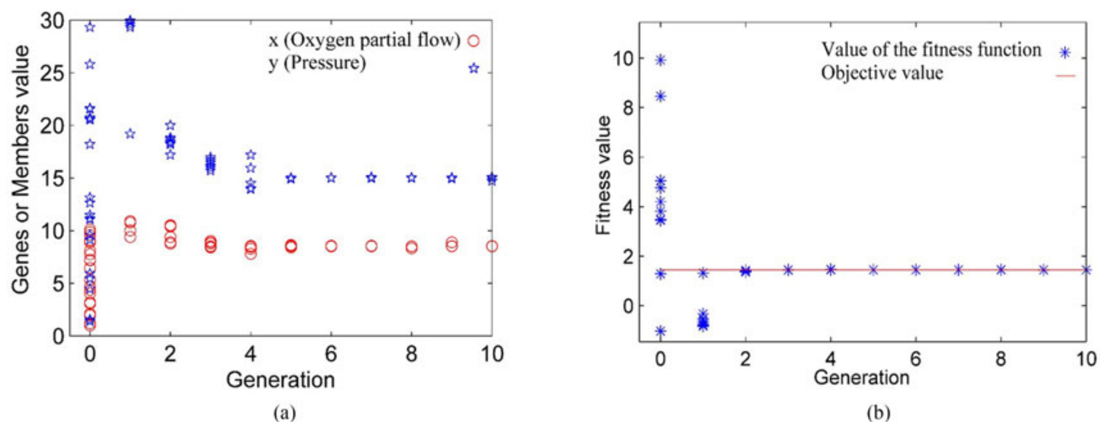

Fig. 5. (a) Genes of all population members at each generation. (b) Evolution of fitness value of population members through the generations for the population size of 20. Blue stars show the value of the fitness function of each member, converging to the objective value (red line).

To further explore the GA's process prediction ability, it was used to find the deposition parameters required to deposit a refractive index that was not experimentally found before. The refractive index of $n = 2.5$ was selected, since it does not exist in Table 1 and since there are no nearby experimentally found refractive indices. The GA predicted the deposition parameters of 10.2% for oxygen partial pressure and 1.7 mTorr pressure. Subsequently the experimentally deposited film measured a refractive index of 2.513 (see Table 5), closely agreeing with the objective value.

4. Fabrication of the Distributed Bragg Reflector

The practicality of the described method was further evaluated by fabricating a Distributed Bragg Reflector (DBR). DBRs, also known as one dimensional photonic crystals, are composed of multi-layers of high and low refractive index (n) materials, where the optical thickness ($n \times thickness$) of each layer is a quarter of reflected wavelength λ_0 (see Fig. 6). The DBR was chosen, because it can be used to validate the ability of the reactive sputtering process to form reliable multi-layers of high and low SiO_x refractive index. The following paragraph describes how the refractive index of each layer influences the reflectivity and bandwidth of a DBR.

When the light is incident on the boundary at which the refractive index changes, it is described by Fresnel law of reflection. However, in the case of a monochromatic plane wave incident to a periodic media like DBR, according to Bloch's theorem, a Bloch wave is generated which takes the periodicity of the one-dimensional lattice. Bloch waves inside the photonic band structure of the periodic media can pass through it only if they are not placed in the band gap of the lattice.

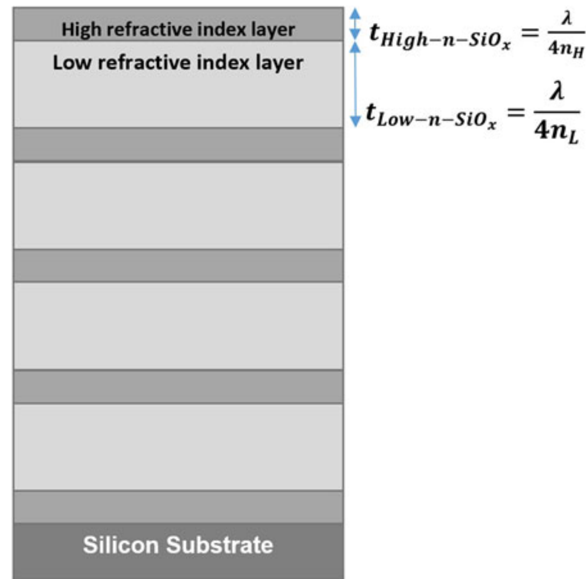

Fig. 6. Schematic of a distributed Bragg reflector consisting of a quarter-wavelength-thick of high and low refractive index SiO_x layers. λ is the central reflected wavelength.

For those electromagnetic waves placed in the band gap, the field energy reflects back which then forms the high reflectivity band of a DBR [30]. DBRs have been used for selectively reflecting of light in surface emitting lasers [31], and LEDs [32], or selecting a special wavelength in photodiodes [33]. The reflection response of a DBR is calculated by (19) [21], [30].

$$\Gamma_1 = \frac{1 - \left(\frac{n_H}{n_L}\right)^{2N} \frac{n_H^2}{n_a n_b}}{1 + \left(\frac{n_H}{n_L}\right)^{2N} \frac{n_H^2}{n_a n_b}} \tag{19}$$

where Γ_1 is the reflectivity, N is the number of layers, n_H and n_L are the high and low refractive indices of the materials, and n_a and n_b are the refractive indices of incident medium and substrate respectively.

The reflected bandwidth is calculated

$$\frac{\Delta\lambda}{\lambda_0} = \frac{\pi}{2}\left[\frac{1}{\cos^{-1}(\rho)} - \frac{1}{\cos^{-1}(-\rho)}\right] \tag{20}$$

where $\rho = \cos(\frac{\delta_H + \delta_L}{2})$, $\delta_H = \frac{2\pi}{\lambda} n_H t_H$, and $\delta_L = \frac{2\pi}{\lambda} n_L t_L$ are the phase thicknesses of the high and low refractive index materials.

As (19) and (20) indicate, for a certain number of layers, a high contrast between the high and low refractive index materials would result in a higher reflectivity as well as higher reflection bandwidth. These are two important characteristics of a DRB. For example, achieving high reflectivity is very important, especially for applications like solar cells where tightly trapping of light is necessary [34].

Depending on the application, several pairs of materials have been used for fabricating DBRs like TiO_2/SiO_2 [35], [36], Ta_2O_5/ SiO_2 [31], [37], Si_3N_4/ SiO_2 [38], AlN/GaN [31], [39], ZnS/CaF_2 [40]. The evaluation DBR of this paper was fabricated by alternately depositing layers of SiO_x with high and low refractive indices, which were determined by the above described GA process. To ensure that the predicted values of GA are robust for fabricating a DBR, the GA was run for 100 times and the average value of the resulted data was recorded. The deposition parameters shown in Table 6 were calculated to fabricate layers of SiO_x with a low refractive index of 1.45 and a high refractive index of 2.5. The DBR was designed based on the standard arrangement of reference

TABLE 6
Fabrication Conditions of the DBR

Layer material	Ar flow	O_2 flow	O_2 partial flow	Pressure	Refractive index
High refractive index SiO_x	34 sccm	2 sccm	5.5%	3.9 mTorr	2.5
Low refractive index SiO_x	56.4 sccm	5.2 sccm	8.4%	17.5 mTorr	1.455

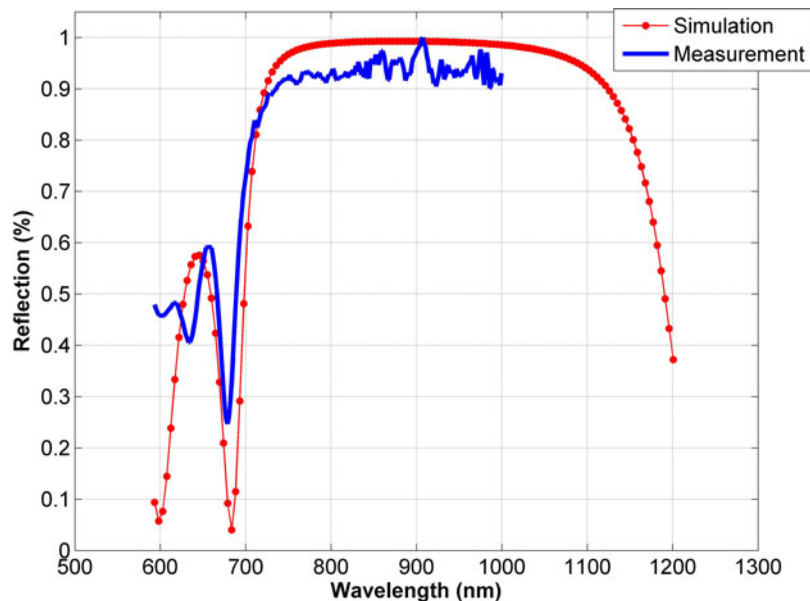

Fig. 7. Calculated (dotted) and measured (solid) spectrum of SiO_x DBR. The graph shows a reflectivity of 95% in reflection-band of more than 270 nm.

[21], consisting of an odd number of layers (9 layers or 4.5 pairs) with the high refractive index layer as the top and bottom layers. The thickness of each layer was based on the quarter wavelength requirement for each layer, which were calculated to be 90 nm for high refractive index ($n = 2.5$) and 155 nm for low refractive index ($n = 1.45$) SiO_x layer, using equations shown in Fig. 6 for a central wavelength of 900 nm. The fabrication conditions are summarized in Table 6.

The reflection profile of the DBR was measured by the ellipsometer operating as a spectrometer, and normalized by the source light intensity. Fig. 7 shows the calculated and measured normalized reflection coefficient of the DBR. From Fig. 7, we can see that the fabricated DBR shows a high reflection of 95%, with the band of high refection wavelengths is extending from 730–1000 nm as measured. The high reflection band theoretically extends beyond the 1000 nm, however, we could not measure this with our spectrometer. The measured data shows some fluctuations within the high reflection band. The reason could be due to the accuracy of the thickness of the deposited SiO_x layers, since if the optical thickness of layers does not exactly match the quarter-wavelength law (see Fig. 6), a portion of the electromagnetic energy at particular wavelengths will be dissipated.

Table 7 shows the features of the DBR fabricated in this work with other DBRs fabricated by sputtering technique, in order to evaluate the fabricated DBR's efficiency. Comparing to works done by [8], [35] and [42], no metal sources were used in the fabrication of this DBR, which is

TABLE 7
Summary of DBR's Characteristics Fabricated by Sputtering Method

Publication	Materials	Fabrication Method	Refractive indices	Reflectivity	Reflection-Band
This work	SiO_x/SiO_x (4.5 pairs)	Reactive RF sputtering	2.5/1.455	> 95%	> 270 nm
F. X. Kärtner *et al.* [35]	TiO_2/SiO_2 (20 pairs)	Ion beam sputtering	2.5/1.5	> 95%	240 nm
S. Chichibu *et al.* [8]	ZrO_2/SiO_2 (8 pairs)	Reactive RF sputtering	2.1/1.46	> 95%	82 nm
M. K. Anuar *et al.* [42]	SiC/MgO (7 pairs)	RF sputtering	3.17/2.19	> 95%	180 nm
C. Levallois *et al.* [43]	a-Si/a-SiN_x (4.5 pairs)	Reactive RF sputtering	3.74/1.84	> 95%	800 nm

important in terms of reducing the losses due to extinction coefficient. The refractive index of SiO_x in the measured range is a real number, which means that the extinction coefficient is almost zero [41], so the losses are negligible [21]. On the other hand, the reactive sputtering of silicon using oxygen is a continuous procedure, so that the DBR can be made using a single material source by simply controlling the system parameters to produce either silicon or SiO_x. An almost similar DBR is fabricated by reference [43] in which SiN_x layers are reactively sputtered from silicon target in the presence of nitrogen gas.

5. Conclusions

This paper investigated the effect of oxygen partial flow and depositing pressure on refractive index of SiO_x thin films deposited by RF reactive magnetron sputtering. A wide range of refractive indices from 1.48–4.28 was shown possible by varying oxygen partial flow between 1–11% for pressure levels from 1.4–17 mTorr. It was found that for a constant amount of oxygen partial flow, the films deposited at the higher pressure range showed a lower refractive index. It was also found that increasing the oxygen partial flow, for a given pressure, reduced the refractive index of deposited film. This reduction was more significant in lower pressures. Experimental data showed that the refractive index of the reactively sputtered SiO_x films could be modeled by only considering the oxygen partial flow and pressure. Statistical modeling from experimental data was used to define a 3-D surface, which was used as the fitness function of the genetic algorithm. The genetic algorithm was employed to determine the required deposition conditions needed to obtain arbitrary refractive indices different from the initial data set. The GA correctly determined needed oxygen partial pressure and process pressure to deposit SiO_x films with a low refractive index of 1.455 and higher index of 2.5. Using the $n = 1.455$ and $n = 2.5$ SiO_x processes, a DBR was fabricated that contained 4.5 pairs of SiO_x layers with high and low refractive indices. The DBR showed a high reflection of 95% in a large bandwidth of more than 270 nm.

References

[1] W. H. Southwell, "Coating design using very thin high- and low-index layers," *Appl. Opt.*, vol. 24, no. 4, pp. 457–460, Feb. 1985.

[2] M. F. Schubert, F. W. Mont, S. Chhajed, D. J. Poxson, J. K. Kim, and E. F. Schubert, "Design of multilayer antireflection coatings made from co-sputtered and low-refractive-index materials by genetic algorithm," *Opt. Exp.*, vol. 16, no. 8, pp. 5290–5298, Apr. 2008.

[3] K. Robbie, "Sculptured thin films and glancing angle deposition: Growth mechanics and applications," *J. Vac. Sci. Technol. A: Vac., Surf., Films*, vol. 15, no. 3, pp. 1460–1465, May 1997.

[4] M. F. Schubert, J. Xi, J. K. Kim, and E. F. Schubert, "Distributed Bragg reflector consisting of high- and low-refractive-index thin film layers made of the same material," *Appl. Phys. Lett.*, vol. 90, no. 14, 2007, Art. no. 141115.

[5] S. Tripathi, S. Maidul Haque, J. S. Misal, D. D. Shinde, K. Divakar Rao, and N. K. Sahoo, "Refractive index tailoring of morphology engineered SiO_2 thin films by collimated glancing angle RF magnetron sputtering," in *Solid State Physics: Proceeding of the 59th DAE Solid State Physics Symposium*, vol. 1665, no. 1, D. Bhattacharyya, Ed. New York, NY, USA: AIP, 2014.

[6] E. Hacker, U. Katenkamp, and H. Fischer, "R.f.-sputtered SiO_2 films for optical applications," *Thin Solid Films*, vol. 97, no. 2, pp. 145–152, Nov. 1982.

[7] W.-F. Wu and B.-S. Chiou, "Optical and mechanical properties of reactively sputtered silicon dioxide films," *Semicond. Sci. Technol.*, vol. 11, pp. 1317–1321, 1996.

[8] S. Chichibu, T. Ohmori, N. Shibata, and T. Koyama, "Dielectric SiO_2/ZrO_2 distributed Bragg reflectors for ZnO microcavities prepared by the reactive helicon-wave-excited-plasma sputtering method," *Appl. Phys. Lett.*, vol. 88, 2006, Art. no. 161914.

[9] V. Bhatt and S. Chandra, "Silicon dioxide films by RF sputtering for microelectronic and MEMS applications," *J. Micromech. Microeng.*, vol. 17, no. 5, pp. 1066–1077, Apr. 2007.

[10] W. Qiu, Y. M. Kang, and L. L. Goddard, "Quasicontinuous refractive index tailoring of SiN_x and SiO_xN_y for broadband antireflective coatings," *Appl. Phys. Lett.*, vol. 96, no. 14, 2010, Art. no. 141116.

[11] S. A. Khodeir and H. M. Sidki, "The effect of the deposition method on the optical properties of SiO_2 thin films," *J. Mater. Sci.: Mater. Electron.*, vol. 12, pp. 107–109, 2001.

[12] A. Palmero, N. Tomozeiu, A. M. Vredenberg, W. M. Arnoldbik, and F. H. P. M. Habraken, "On the deposition process of silicon suboxides by a RF magnetron reactive sputtering in Ar–O_2 mixtures: Theoretical and experimental approach," *Surf. Coating Technol.*, vol. 177/178, pp. 215–221, Jan. 2004.

[13] S. Maniv and W. D. Westwood, "Oxidation of an aluminum magnetron sputtering target in Ar/O_2 mixtures," *J. Appl. Phys.*, vol. 51, no. 1, pp. 718–725, 1980.

[14] H. Bartzsch and P. Frach, "Modeling the stability of reactive sputtering processes," *Surf. Coating Technol.*, vol. 142–144, pp. 192–200, Jul. 2001.

[15] T. Kubart, O. Kappertz, T. Nyberg, and S. Berg, "Dynamic behavior of the reactive sputtering process," *Thin Solid Films*, vol. 515, no. 2, pp. 421–424, Oct. 2006.

[16] O. Auciello and A. R. Krauss, "In situ real-time characterization of thin films," *Meas. Sci. Technol.*, vol. 13, no. 4, pp. 644–644, Mar. 2002.

[17] N. Tomozeiu, J. Van Hapert, E. Van Faassen, W. Arnoldbik, A. Vredenberg, and F. Habraken, "Structural properties of a-SiO_x layers deposited by reactive sputtering technique," *J. Optoelectron. Adv. Mater.*, vol. 4, pp. 513–521, 2002.

[18] E. Van Hattum, A. Palmero, W. Arnoldbik, and F. Habraken, "Experimental characterization of the deposition of silicon sub oxide films in a radiofrequency magnetron reactive sputtering system," *Surf. Coating Technol.*, vol. 188, pp. 399–403, 2004.

[19] L.-N. He and J. Xu, "Properties of amorphous SiO_2 films prepared by reactive RF magnetron sputtering method," *Vacuum*, vol. 68, pp. 197–202, 2002.

[20] H. Fujiwara, "Data analysis," in *Spectroscopic Ellipsometry: Principles and Applications*. Chichester, U.K.: Wiley, 2007.

[21] S. J. Orfanidis, "Multilayer structures," in *Electromagnetic Waves and Antennas*. New Brunswick, NJ, USA: Rutgers Univ. Press, 2002.

[22] R. Valletta, J. Perri, and J. Riseman, "Reactively sputtered silicon dioxide films," *Electrochem. Technol.*, vol. 4, pp. 402–406, 1966.

[23] H.-C. Lin, C.-T. Su, C.-C. Wang, B.-H. Chang, and R.-C. Juang, "Parameter optimization of continuous sputtering process based on Taguchi methods, neural networks, desirability function, and genetic algorithms," *Expert Syst. Appl.*, vol. 39, no. 17, pp. 12918–12925, Dec. 2012.

[24] W.-H. Ho, J.-T. Tsai, G.-M. Hsu, and J.-H. Chou, "Process parameters optimization: A design study for TiO_2 thin film of vacuum sputtering process," *IEEE Trans. Autom. Sci. Eng.*, vol. 7, no. 1, pp. 143–146, Jan. 2010.

[25] M. Sivapragash, P. Kumaradhas, B. S. Jones Retnam, X. F. Joseph, and U. T. S. Pillai, "Taguchi based genetic approach for optimizing the PVD process parameter for coating ZrN on AZ91D magnesium alloy," *Mater. Des.*, vol. 90, pp. 713–722, Jan. 2016.

[26] C. R. Houck, J. Joines, and M. G. Kay, "A genetic algorithm for function optimization: A MATLAB implementation," North Carolina State Univ., Raleigh, NC, USA, *NCSU-IE TR 95-09*, 1995.

[27] K. Deb, "An efficient constraint handling method for genetic algorithms," *Comput. Methods Appl. Mech. Eng.*, vol. 186, pp. 311–338, 2000.

[28] J. J. Grefenstette, "Optimization of control parameters for genetic algorithms," *IEEE Trans. Syst., Man, Cybern.*, vol. SMC-16, no. 1, pp. 122–128, Jan. 1986.

[29] J. D. Schaffer, R. A. Caruana, L. J. Eshelman, and R. Das, "A study of control parameters affecting online performance of genetic algorithms for function optimization," in *Proc. 3rd Int. Conf. Genetic Algorithms*, 1989, pp. 51–60.

[30] P. Yeh, "Optics of periodic layered media," in *Optical Waves in Layered Media*. Chichester, U.K.: Wiley, 2005.

[31] C.-C. Kao *et al.*, "Fabrication and performance of blue GaN-based vertical-cavity surface emitting laser employing AlN/GaN and Ta_2O_5/ SiO_2 distributed Bragg reflector," *Appl. Phys. Lett.*, vol. 87, no. 8, 2005, Art. no. 081105.

[32] T. Kato *et al.*, "GaAs/GaAlAs surface emitting IR LED with Bragg reflector grown by MOCVD," *J. Cryst. Growth*, vol. 107, pp. 832–835, Jan. 1991.

[33] J. Dai *et al.*, "Design and fabrication of UV band-pass filters based on SiO_2/Si_3N_4 dielectric distributed Bragg reflectors," *Appl. Surf. Sci.*, vol. 364, pp. 886–891, Feb. 2016.

[34] L. Zeng *et al.*, "Efficiency enhancement in Si solar cells by textured photonic crystal back reflector," *Appl. Phys. Lett.*, vol. 89, 2006, Art. no. 111111.

[35] F. X. Kärtner *et al.*, "Design and fabrication of double-chirped mirrors," *Opt. Lett.*, vol. 22, no. 11, pp. 831–833, Jun. 1997.

[36] S. Valligatla *et al.*, "High quality factor 1-D $Er3+$-activated dielectric microcavity fabricated by RF-sputtering," *Opt. Exp.*, vol. 20, pp. 21214–21222, Aug. 2012.

[37] R. Horng, W.-K. Wang, S.-Y. Huang, and D.-S. Wuu, "Effect of resonant cavity in wafer-bonded green InGaN LED with dielectric and silver mirrors," *IEEE Photon. Technol. Lett.*, vol. 18, no. 3, pp. 457–459, Feb. 2006.

[38] H. J. Lee, "Techniques for fabricating Bragg reflectors on SiO_2–Si_3N_4–SiO_2 rib waveguides on Si," *Appl. Opt.*, vol. 27, no. 6, pp. 1199–1202, Mar. 1988.
[39] H. H. Yao, C. F. Lin, H. C. Kuo, and S. C. Wang, "MOCVD growth of AlN/GaN DBR structures under various ambient conditions," *J. Cryst. Growth*, vol. 262, no. 1–4, pp. 151–156, Feb. 2004.
[40] M. Muallem, A. Palatnik, G. D. Nessim, and Y. R. Tischler, "Room temperature fabrication of dielectric Bragg reflectors composed of a CaF_2 /ZnS multilayered coating," *ACS Appl. Mater. Interfaces*, vol. 7, no. 1, pp. 474–481, Jan. 2015.
[41] E. D. Palik and G. Ghosh, "Refractive index," in *Electronic Handbook Of Optical Constants Of Solids: V1-5*. San Diego, CA, USA: Academic, 1999.
[42] M. K. Anuar *et al.*, "Development of SiC/MgO distributed Bragg reflector using RF magnetron sputtering technique," in *Proc. IEEE Int. Conf. Semicond. Electron.*, 2006, pp. 378–381.
[43] C. Levallois *et al.*, "Design and fabrication of GaInAsP/InP VCSEL with two a-Si/a-SiNx Bragg reflectors," *Opt. Quantum Electron.*, vol. 38, pp. 281–291, 2006.